ADVANCED MATERIALS TECHNOLOGIES
www.advmattechnol.de

Spatially Controlled 3D Printing of Dual-Curing Urethane Elastomers

*Brian M. Howell, Caitlyn C. Cook, Michael D. Grapes, Karen Dubbin, Emily L. Robertson, John D. Sain, Kyle T. Sullivan, Eric B. Duoss, and Eric V. Bukovsky**

3D printing of functional materials with spatial control of structure and composition is useful for many applications and increases design space. Here, a microextrusion-based method, known as direct ink writing (DIW), is harnessed to further advance 3D complexity by tuning dual-cure ink formulations via varying fillers and filler concentrations. In these inks, low-molecular-weight minor acrylate components enable printing of complex shapes by rapid UV curing during printing while the major heat-cured urethane components provide elastomeric properties when forming a urethane-grafted acrylate polymer (UGAP). The printing process itself displays exquisite control of structure and composition as well as robustness to inks exhibiting a wide range of yield stresses (between 11.5 and 8042 Pa) while still maintaining necessary shape retention during printing. By incorporating micro- or nanosized solid fillers in the inks, an expansive range of both structural and mechanical properties are achievable. Additionally, by modulating the ratio of resin and solid fillers, various combinations of print-mold and pore-forming steps can be employed to expand the design space. The power and versatility of these process permutations are demonstrated by producing a broad range of complex components with controlled properties and performance for applications such as soft robotics.

1. Introduction

Additive manufacturing (AM) processes are pushing design into previously impossible geometries with advanced and multifunctional materials triggering disruptive (albeit positive) shifts in the techno-socioeconomic landscape.[1–5] The ever-increasing 3D complexity of objects is driving development of new AM techniques,[6–8] increasing spatial and compositional control across multiple orders of length scale.[9,10] Direct ink writing (DIW) extends this feat by extruding shear thinning viscoelastic fluids that exhibit shape retention when the shear strain is dramatically reduced after deposition from the nozzle, thus allowing for ink composition flexibility to encompass a wide range of mechanical properties.[11,12] However, materials with poor hysteretic recovery or low yield stresses can limit spatial precision for complex print patterns (e.g., spanning gaps). To address these difficulties, recent published methods utilized various mechanisms to aid in filament shape retention while maintaining desired material properties. For example, embedded printing methods enable freeform printing within support-bath material that provides buoyant forces to stabilize the deposited filaments.[10] Other approaches include the use of multimaterial 3D printing for fine compositional tuning within printed materials in which scaffolding material can be precisely deposited, or manipulating an electromagnetic field to control the placement of inks doped with ferromagnetic particles.[13,14]

On-demand UV curing has further improved spatial resolution of DIW by rapidly modifying ink rheology, typically through the addition of acrylate functional groups and a photoinitiator.[15–17] Past attempts with rapid UV curing, however, have resulted in brittle and rigid mechanical properties due to high concentrations of low-molecular-weight monomers in the ink formulations.[15] Additionally, on-demand UV curing has reduced interfacial strength between filaments resulting in anisotropic mechanical properties depending on print orientation.[15,18] This occurs as a result of uncontrolled rapid UV kinetics reaching gelation to rapidly to enable subsequent interfilament bonding, or, the formulation is too sensitive to UV light upon exiting the nozzle. Dual-curing efforts have shown promise in controlling the extent of UV-curable components to allow sufficient stiffening when printing while accessing mechanical properties inherent to tough epoxies.[15,19–21]

Here we expand this dual-curing approach to a urethane-grafted acrylate polymer (UGAP) in order to exploit the rheological flexibility provided by on-demand curing. Elastomeric mechanical properties provided by combinations of urethane and acrylate components and leaching of solid filler[22–24] produce a material that accesses previously unattainable structures often required for application spaces such as soft robotics, functional materials, and biomedical devices.[25–28]

B. M. Howell
Mechanical Engineering Department
University of California
Berkeley, CA 94720, USA

B. M. Howell, C. C. Cook, M. D. Grapes, K. Dubbin, E. L. Robertson, J. D. Sain, K. T. Sullivan, E. B. Duoss, E. V. Bukovsky
Lawrence Livermore National Laboratory
Livermore, CA 94550, USA
E-mail: bukovsky1@llnl.gov

The ORCID identification number(s) for the author(s) of this article can be found under https://doi.org/10.1002/admt.202100700.

DOI: 10.1002/admt.202100700

2. Results and Discussion

We demonstrate the UGAP ink's versatility in a combination of complex printing motifs to manufacture objects exhibiting a range of mechanical properties while maintaining spatial print control. On-demand UV exposure chemically bonds the minor concentration of low-molecular-weight acrylate monomer, ethylene glycol phenyl ethyl acrylate (EGPEA), and 1,6-hexanediol diacrylate (HDDA), to the backbone of an isocyanate, acrylate-functionalized prepolymer (EBECRYL 4396) to provide sufficient shape retention through stiffening, while maintaining interfilament adhesion. A subsequent postprocess thermal-curing step forms the dominant urethane network comprised of polycaprolactone diol (8025D) and triol (8025E) bonded to the isocyanates of EBECRYL 4396 without disrupting the printed shape. The optimized formulation using 16.67 wt% low-molecular-weight acrylate and 3.33 wt% diphenyl(2,4,6-trimethylbenzoyl)phosphine oxide (Irgacure 819) was formulated based on sag testing that can be found in Figure S1 (Supporting Information), where increasing the acrylate diluents decreased ink yield stress and increased sagging. While the increase in acrylate should have made the filaments more rigid during UV-light-induced curing, the low viscosity of the low-molecular-weight acrylates significantly reduced the overall ink viscosity resulting in the opposite effect, causing sagging before the ink could attain sufficient gelation to halt sagging. Polyol components and corresponding ratios were chosen to maximize the crosslink density while forming a stoichiometric ratio with the isocyanates in the UGAP prepolymer. Rheology of UGAP formulations (Table S1, Supporting Information) was varied by concentrations of either fumed silica (UGAP-FS) or NaCl (UGAP-NaCl) fillers. Mechanical testing was performed on UGAP-FS type IV dog bones designed with directionally dependent toolpaths (Figure S2A, Supporting Information) to evaluate effects from filament–filament adhesion. The resulting stress–strain curves and the tensile modulus indicated that in situ curing of the UGAP ink still allowed sufficient interfilament adhesion such that printing orientation did not result in anisotropic material properties (Figure S2B, Supporting Information) as indicated in past work.[15] Alternative fillers such as alumina were also found to be easily incorporated into the UGAP base resin due to the use of acrylate diluents (Figure S3, Supporting Information).

The UV curing relaxes the rheological and dimensional constraints of postextruded ink required for geometrically complex objects (**Figure 1**A). By increasing filament stiffness during

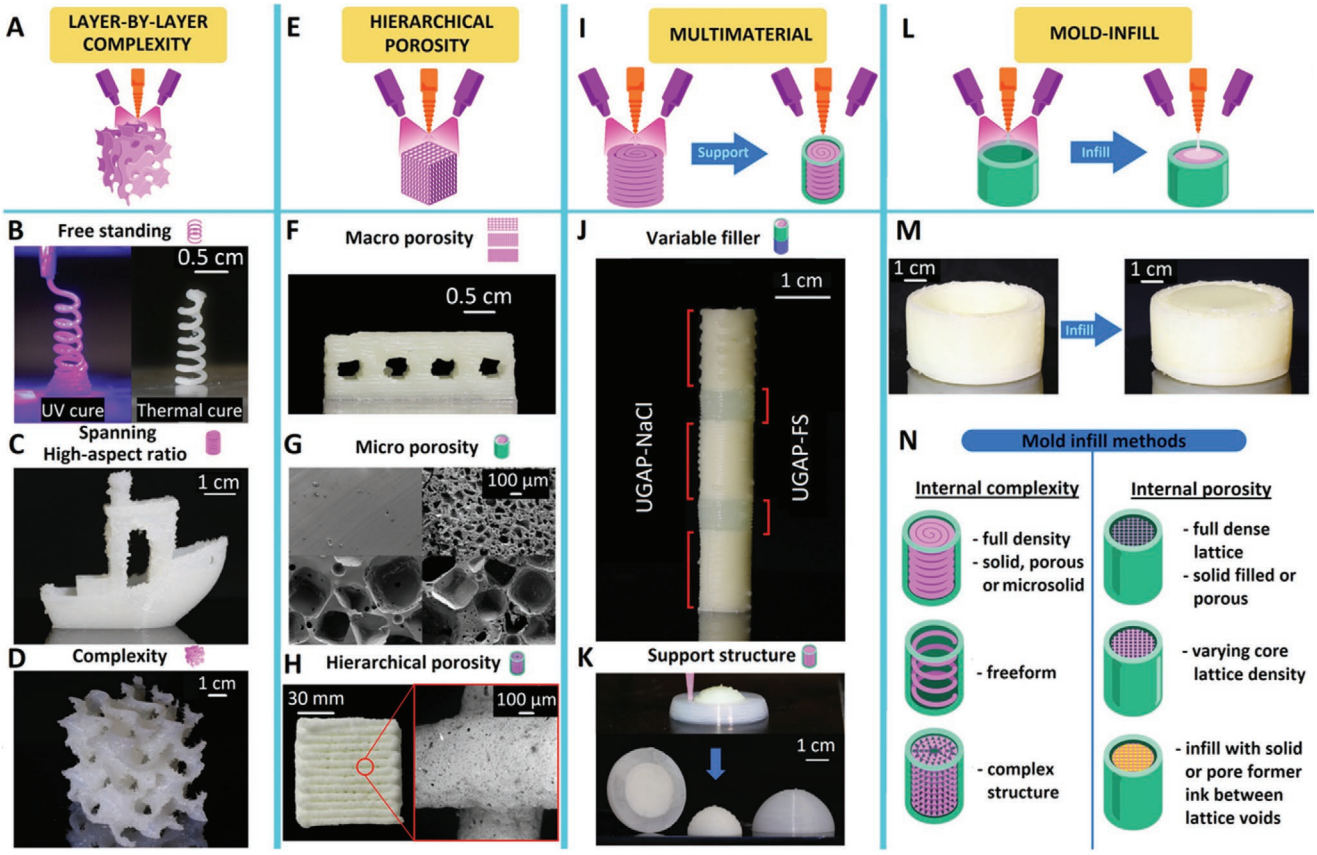

Figure 1. Schematic of possible printing combinations with UGAP DIW printing. A) Layer-by-layer complexity via intermediate UV cure. B) Millimeter scale helix. C) 3D Benchie. D) Gyroid printed using UGAP inks filled with fumed silica (UGAP-FS). E) Porosity on variable length scales. F) Designed macroporosity. G) Scanning electron microscopy (SEM) images of microporosity produced by leaching NaCl particles. H) Hierarchical combination of macro- and microporosity. I) Multimaterial printing. J) A cylinder co-printed, UGAP-NaCl, and 10 wt% UGAP-FS. K) UGAP-FS support structure for silicone ink. L) Infill fabrication for M) printing an outer mold and filling to full density. N) Multiple methods of printing an outer shell with various internal structure.

printing, shape retention is maintained allowing for unsupported printing in free space of a multi-millimeter-scale helix (Figure 1B). Rapid stiffening also extended printing scales permitting large-format and high-aspect-ratio designs like the 3D Benchy (Figure 1C), a notoriously difficult-to-print benchmark for fused-deposition modeling as well as the steep overhangs required for a gyroid (Figure 1D). Structural composition control (Figure 1E) was achieved through macroscopic voids from toolpath variations (Figure 1F) and microscopic voids through postprocess leaching of NaCl resulting in microscopic pores patterned by NaCl loading and particle size distribution (Figure 1G; Figure S4, Supporting Information).[29] The combination of spatial print control and solids' leaching methodologies allowed structures exhibiting hierarchical porosity (Figure 1H) forming porous UGAP (UGAP-pore). Utilizing multimaterial printing[13,30] (two different UGAP-based inks) significantly expanded the application space allowing for property localization throughout the part (Figure 1I). Concurrent printing of UGAP-FS or UGAP-NaCl inks produced structures with spatially resolved mechanical responses that were chemically bonded forming a resilient composite (Figure 1J). UGAP-based inks further expanded the fabrication space as support material for inks ill-suited for DIW techniques (Figure 1K). Modulating the UV light intensity and exposure allows spatiotemporal control of printed filament stiffness throughout the toolpath such that shape retention and volume filling behavior can be utilized in the same print (Figure 1L,M). Such a range of utility permits a variety of printing motifs (Figure 1N) and complex internal architectures.

Incorporating the minor acrylate components EGPEA, HDDA, and including the acrylate groups on the EBECRYL 4396 not only assists in on-demand UV curing of complex shapes but also enables printing of a wide range of ink yield stresses. The 70 wt% micrometer-scale bimodal distribution of NaCl in UGAP-NaCl and increasing nanoscale silica content from 5 to 15 wt% in UGAP-FS created a family of ink that ranged in yield stress from 11.5 and 8042 Pa (**Figure 2**A). When printed without UV light, filaments of the lower yield stress ink UGAP-NaCl (11.5 Pa) collapsed along the central axis due to the weight of successive layers (Figure 2B). Conversely, the higher yield stress of 15 wt% UGAP-FS (8042 Pa) allowed taller lattices to be printed without UV light. However, even the 15 wt% UGAP-FS high-aspect-ratio tower collapsed midprint due to lateral loads created by the *X Y* printing stage during printing. With on-demand UV exposure, the same tower was printed with both UGAP-NaCl and 15 wt% UGAP-FS to the physical limits of our printer (8.7 cm in height) with minimal dimensional differences between the two parts (dimensional comparison shown Figure S5 in the Supporting Information). As shown, NaCl and silica UGAP inks all demonstrated successful DIW printing despite the quantified rheological differences.

On-demand UV curing during printing enabled rapid stiffening of the minor acrylate component, the cure kinetics of which were characterized with UV-dependent rheology. UGAP-NaCl UV rheology results demonstrate the rapid kinetics with increasing light intensity (Figure 2C), attaining a full-depth cure within 60 s with 0.6 mW cm^{-2} flood exposure. For a printing speed of 15 mm s^{-1}, sufficient stiffening was observed within ≈10 s of UV exposure creating optimum filament–filament adhesion and shape retention. This observation indicates a lack of full filament depth cure caused by solid-filler-induced light scattering. Full acrylate cure originates from surface cure (Figure S6, Supporting Information) relying on chain-growth radical-based kinetics to propagate toward the filament core where the UV light could not penetrate (Figure S7, Supporting Information). Further UV-rheology cure and depth analysis are discussed in the Supporting Information. The rapid filament stiffening allowed parts with filament overhangs (i.e., hollow cone with each subsequent layer off-set by half filament) to be printed with UGAP-NaCl and 15 wt% UGAP-FS (Figure 2D). Filament gap spanning tests (Figure 2E) further confirmed that the stiffening rate due to UV exposure at the 15 mm s^{-1} print speed was sufficient as the low yield stress UGAP-NaCl formulation was able to span the largest 10 mm gap with only minor sag when exposed to UV light. Conversely, the UGAP-FS inks were able to span the increasing gaps with and without the aid of the UV light. The UGAP-NaCl and 15 wt% UGAP-FS performed similarly when printing overhangs with UV light. Figure 2F shows an inverted pyramid with each side having different angles to demonstrate sag resistance in an overhang. In all cases, postprinting thermal curing of the major urethane component at 80 °C did not exhibit dimensional changes indicating that a suitably crosslinked matrix created from UV-induced curing was stable enough to resist thermal-induced dimensional change. Fourier transform IR (FTIR) characterization indicates complete conversion of acrylate and urethane components (Figure S8, Supporting Information), while dynamic mechanical analysis (DMA) reveals a single but somewhat broad glass transition temperature (T_g) peak centered at −25 °C to signify a fully covalently linked UGAP elastomer network (Figure S9, Supporting Information).

While the elastomeric mechanical properties are dictated by the thermal curing of the major urethane prepolymer component, modifying filler and filler concentrations provided tunable stiffness control. Comparing compression moduli of 15 wt% UGAP-FS to 70 wt% UGAP-NaCl printed lattices showed a 1.5 times lower modulus in UGAP-FS filled parts to that of UGAP-NaCl, going from 1.24 to 0.80 MPa, respectively (Figure 2G). Since the polycaprolactone urethane prepolymer used in UGAP allowed for the cured network to be water permeable, the NaCl filler was gravimetrically extractable with water postprinting and curing. While leaching solid fillers from a cured composite matrix to pattern voids inside the matrix is not new, it is a useful postprocessing step for these UGAP inks affording greater tunability in the mechanical properties of the final part. UGAP-pore lattice compression modulus was 3.4 times lower than the NaCl counterpart with a modulus of 0.37 MPa due to the resultant porous microstructure. UGAP-NaCl and UGAP-pore lattices are shown in Figure 2H withstanding a 5 N load demonstrating increased compressibility due to the porous microstructure, while UGAP-pore lattices exhibited repeated compression without permanent deformation (Figure S10, Supporting Information). The large range in compressive moduli within the same polymeric network provides opportunities for localized control of mechanical responses required in functional materials not possible with traditional DIW.

Elastomeric and functional materials are showing greater promise for soft-robotic applications. Shape memory motion

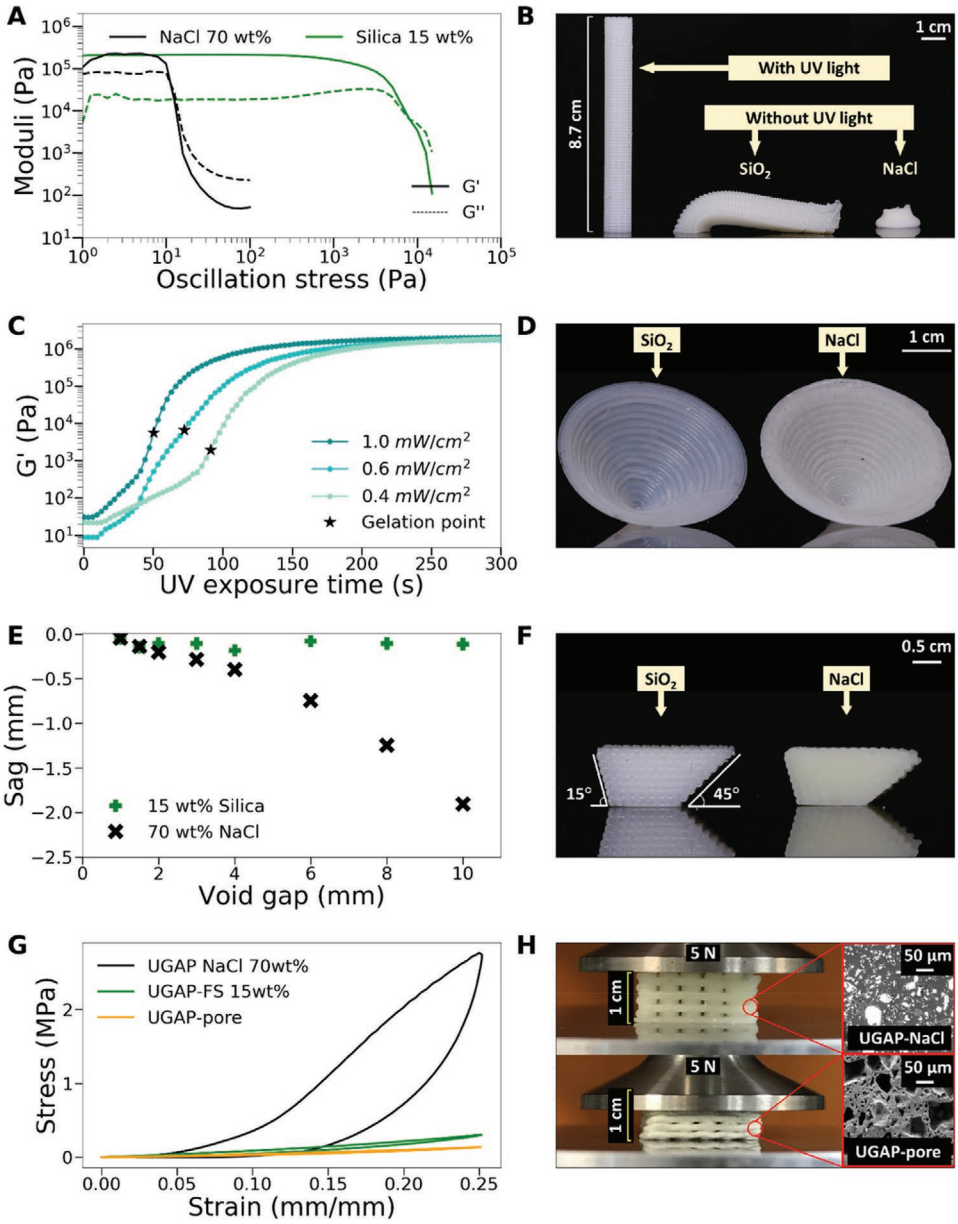

Figure 2. A) Yield stress comparison of UGAP resins filled with 70 wt% NaCl and 15 wt% fumed silica. B) 1 cm × 1 cm towers printed as tall as possible with UGAP-NaCl and UGAP-FS with and without UV light. C) UV-rheology storage modulus for UGAP-NaCl with increasing light intensity. D) Hollow cones with UGAP-NaCl and 15 wt% UGAP-FS demonstrating overhangs. E) Spanning tests measuring sag distance for UGAP inks. F) Inverted pyramids with 15° and 45° side angles printed with UGAP-NaCl and UGAP-FS. G) Printed lattices withstanding 25% strain. H) Static 5 N loading on UGAP-NaCl and UGAP-pore lattices with same filament spacing, SEM images of UGAP-NaCl, and UGAP-pore samples.

of elastomeric materials is triggered by heating past the T_g of the elastomer.[31] At temperatures above the T_g, a material can be placed into a desired configuration and be programmed by cooling below the T_g. The material will remain in this programmed state until heated through its T_g, at which time it will return to its original shape. Demonstrating this phenomenon with UGAP-FS, a printed gripper (**Figure 3**A) is shown actuating from the programmed state (holding a ball) to the original shape, releasing the ball. To demonstrate more complex print structures, a co-printed soft–hard segmented finger was designed containing in-fill motifs outlined in Figure 1J. To simulate the motion of an opening finger, three sections of the finger were printed with varying lattice densities with UGAP-pore to modulate flexibility separated by two fully dense joints using UGAP-FS. The hierarchical structure of the pores facilitated the variation of compressibility (Figure 3B) allowing for segmented flexibility during actuation. Actuation was achieved by heating the entire part from the programmed state (curled) to the original state (straight). As shown in Figure 3C, the degree of flex between each joint was limited by the macroporosity dictated by the in-filled lattice density. In a final dimension of this work, it was found that the UGAP-pore microstructure

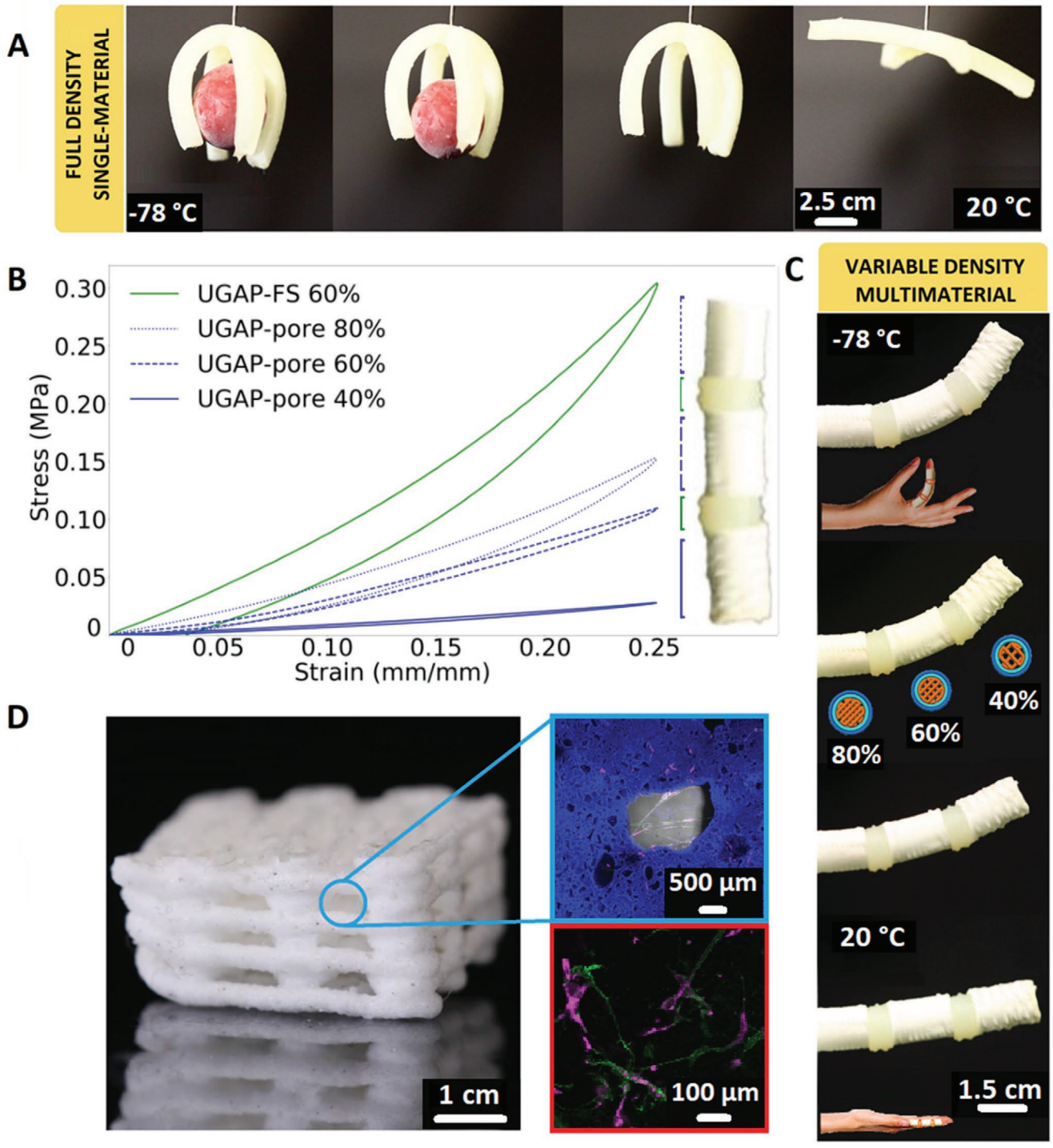

Figure 3. A) Printed gripper holding ball in "programmed" configuration and releasing to the original configuration with heating. B) Compressive mechanical properties of inks in multimaterial cylinder UGAP-pore with lattice densities of 40%, 60%, and 80% and UGAP-FS segments. C) Multimaterial cylinder in the programmed state actuating to the original state. D) Printed porous structures facilitating the growth of human lung fibroblasts. Fluorescence microscope image showing the microporous background (blue), fibroblast cell membrane stain (pink), and the actin stain (green).

facilitated growth of human lung fibroblasts (Figure 3D) indicating that UGAP could potentially be used as an environment for cell growth in future work and serve as a framework for actuating scaffolds for biological applications.

3. Conclusion

Introducing spatial control using a dual-cure low-molecular-weight acrylate component UGAP ink is a significant

advancement for DIW, demonstrating a previously unattainable broad range of printing motifs with tunable elastomeric properties. The acrylate diluent afforded lower initial ink viscosities, and, with the assistance of on-demand UV curing, a wide range of rheological yield stress inks ranging from 11.5 Pa (UGAP-NaCl) to 8042 Pa (UGAP-FS 15 wt%) was successfully printed. Rapid stiffening with UV light exposure allowed for near instantaneous rheology modification and shape retention in this range of printable inks, maintaining dimensional print accuracy for complex prints such as free form helices, gyroids, and lattice towers reaching the *z*-height limit of the printer. Characterization of the UV-curing kinetics allowed finer tuning of spatial print control with on-demand printing by tuning the light exposure intensity and understanding the extent of dark-cure polymerization. Since previous acrylate-based UV-curable DIW inks exhibited more brittle-like mechanical properties or poor interfilament adhesion, developing the UGAP ink with a minor concentration of acrylate diluent crosslinked with a major urethane component provided parts with elastomeric properties and robust interfilament bonding. The resultant compression moduli of filled printed lattice parts spanned an order of magnitude, from 1.24 MPa in UGAP-NaCl parts to 0.80 MPa in UGAP-FS and further tuning to 0.37 MPa of UGAP-pore by leaching out NaCl. This mechanical property range within the same base UGAP ink in conjunction with the low elastomeric T_g provides shape memory material properties, setting the stage for applications in soft robotics, which was also successfully demonstrated. Achieving spatial print control in DIW inks with superior and tunable elastomeric properties raises the benchmark for future UV-curable ink formulations and opens the door to increasing the functionality in printed applications.

4. Experimental Section

Materials: Polycaprolactone diol (8025D) and triol (8025E) (Perstorp Chemical, M_W = 2000 g mol^{-1}, OH equiv. = 56 and 84 mg g^{-1}, respectively), polyisocyanates/acrylate (EBECRYL 4396, Allnex USA Inc., NCO = 7.5 wt%, acrylate = 1 equiv.), EGPEA, HDDA, Irgacure 819 (Sigma Aldrich), and fumed silica (Aerosil R202, Evonik) were used as received. NaCl (Sigma Aldrich) was ground in a Retsch RM 200 automatic mortar and pestle, and sieved to course (75–106 micron) and fine (<45 micron) size distributions. NaCl powders were then dried at 100 °C for 1 h and were stored in a desiccator until used.

Ink Formulation: UGAP components (40.84 wt% 8025D, 35.07 wt% EBECRYL 4396, 15 wt% EGPEA, 4.08 wt% 8025E, 3.33 wt% Irgacure 819, and 1.67 wt% HDDA) were mixed in a Flacktek DAC 150.1 FV-K SpeedMixer for 60 s intervals at 2000 rpm, ensuring that the temperature did not exceed 35 °C. Refer to Table S1 (Supporting Information) for explicit formulations.

Ink Rheology and UV Sensitivity: Oscillatory rheology was performed on a TA Instruments AR2000Ex rheometer. A 25 mm Peltier parallel plate, with a sample thickness of 1.5 mm and a constant frequency of 1 Hz was used for stress sweeps. For UV rheology experiments, 0.840 mm thick samples were exposed (S2000, Omnicure, 400–500 nm filter, spectrum; Figure S11, Supporting Information) between a 20 mm aluminum upper plate and 20 mm acrylic lower plate. A linear viscoelastic regime was found using a 0.5% strain and a 1 rad s^{-1} oscillation frequency.

Printing: Prepared inks were loaded into Nordson optimum UV-blocking 30 cc syringes with an optimum syringe piston and 0.840 mm tapered nozzle wrapped in Kapton tape. Samples were degassed in the Flacktek for 2 min at 3500 rpm. An air-powered fluid dispenser (Ultimus V, Nordson EFD) was used to extrude the ink. UV light was generated by an Omnicure S2000 lamp with a 400-500 nm filter lamp through three probes attached to a custom-designed mount (refer to Figure S12 in the Supporting Information for a schematic). An Aerotech ANT 130-XY and 130-L-Z5 axis stage was controlled via an A3200 controller through an Aerotech A3200 CNC operator interface (v.5.05.000). Gravimetric removal of sodium chloride (solids leaching) was performed by stirring parts in a covered container of distilled water at 80 °C until NaCl was removed.

Mechanical Testing: Spanning tests were performed on custom blocks with increasing voids (Figure S13, Supporting Information) based on a procedure from Smay et al.[32] Sag distance was measured with a Keyence One-shot 3D Measurement Macroscope VR-3200. The surface of each sample was sprayed with zinc stearate to dull the reflection. Compression specimens were tested on an Instron 5943 equipped with a 1 kN load cell. Tensile samples were tested under uniaxial loading.

Supporting Information

Supporting Information is available from the Wiley Online Library or from the author.

Acknowledgements

The authors gratefully acknowledge Melody Golobic for training and use of the DIW printer. This work was performed under the auspices of the U.S. Department of Energy by Lawrence Livermore National Laboratory under Contract DE-AC52-07NA27344. LLNL-JRNL-821072.

Conflict of Interest

The authors declare no conflict of interest.

Data Availability Statement

The data that support the findings of this study are available from the corresponding author upon reasonable request.

Keywords

additive manufacturing, direct ink write, dual cure, elastomer, polyurethane

Received: June 11, 2021
Revised: August 28, 2021
Published online: October 10, 2021

[1] N. Li, S. Huang, G. Zhang, R. Qin, W. Liu, H. Xiong, G. Shi, J. Blackburn, *J. Mater. Sci. Technol.* **2019**, *35*, 242.
[2] P. Parandoush, D. Lin, *Compos. Struct.* **2017**, *182*, 36.
[3] D.-G. Shin, T.-H. Kim, D.-E. Kim, *Int. J. Precis. Eng. Manuf. - Green Technol.* **2017**, *4*, 349.
[4] X. Wang, M. Jiang, Z. Zhou, J. Gou, D. Hui, *Composites, Part B* **2017**, *110*, 442.
[5] F. Caviggioli, E. Ughetto, *Int. J. Prod. Econ.* **2019**, *208*, 254.
[6] B. E. Kelly, I. Bhattacharya, H. Heidari, M. Shusteff, C. M. Spadaccini, H. K. Taylor, *Science* **2019**, *363*, 1075.

[7] X. Zheng, H. Lee, T. H. Weisgraber, M. Shusteff, J. DeOtte, E. B. Duoss, J. D. Kuntz, M. M. Biener, Q. Ge, J. A. Jackson, S. O. Kucheyev, N. X. Fang, C. M. Spadaccini, *Science* **2014**, *344*, 1373.
[8] X. Peng, X. Kuang, D. J. Roach, Y. Wang, C. M. Hamel, C. Lu, H. J. Qi, *Addit. Manuf.* **2021**, *40*, 101911.
[9] M. Wehner, R. L. Truby, D. J. Fitzgerald, B. Mosadegh, G. M. Whitesides, J. A. Lewis, R. J. Wood, *Nature* **2016**, *536*, 451.
[10] D. J. Shiwarski, A. R. Hudson, J. W. Tashman, A. W. Feinberg, *APL Bioeng.* **2021**, *5*, 010904.
[11] Q. Chen, P.-F. Cao, R. C. Advincula, *Adv. Funct. Mater.* **2018**, *28*, 1800631.
[12] Q. Zhang, D. Lin, B. Deng, X. Xu, Q. Nian, S. Jin, K. D. Leedy, H. Li, G. J. Cheng, *Adv. Mater.* **2017**, *29*, 1605506.
[13] M. A. Skylar-Scott, J. Mueller, C. W. Visser, J. A. Lewis, *Nature* **2019**, *575*, 330.
[14] D. Kokkinis, M. Schaffner, A. R. Studart, *Nat. Commun.* **2015**, *6*, 8643.
[15] K. Chen, X. Kuang, V. Li, G. Kang, H. J. Qi, *Soft Matter* **2018**, *14*, 1879.
[16] L. L. Lebel, B. Aissa, M. A. E. Khakani, D. Therriault, *Adv. Mater.* **2010**, *22*, 592.
[17] G. Griffini, M. Invernizzi, M. Levi, G. Natale, G. Postiglione, S. Turri, *Polymer* **2016**, *91*, 174.
[18] G. Postiglione, G. Natale, G. Griffini, M. Levi, S. Turri, *Polym. Compos.* **2017**, *38*, 1662.
[19] T. Wu, P. Jiang, X. Zhang, Y. Guo, Z. Ji, X. Jia, X. Wang, F. Zhou, W. Liu, *Mater. Des.* **2019**, *180*, 107947.
[20] Q. Chen, T. Sukmanee, L. Rong, M. Yang, J. Ren, S. Ekgasit, R. Advincula, *ACS Appl. Polym. Mater.* **2020**, *2*, 5492.
[21] Z. Jiang, B. Diggle, M. L. Tan, J. Viktorova, C. W. Bennett, L. A. Connal, *Adv. Sci.* **2020**, *7*, 2001379.
[22] X. Mu, T. Bertron, C. Dunn, H. Qiao, J. Wu, Z. Zhao, C. Saldana, H. J. Qi, *Mater. Horiz.* **2017**, *4*, 442.
[23] N. Kleger, M. Cihova, K. Masania, A. R. Studart, J. F. Löffler, *Adv. Mater.* **2019**, *31*, 37.
[24] A. E. Jakus, N. R. Geisendorfer, P. L. Lewis, R. N. Shah, *Acta Biomater.* **2018**, *72*, 94.
[25] N. Farokhnia, A. Caprio, V. Kashyap, S. Al'Aref, L. Baskaran, B. Mosadegh, S. Dunham, *Adv. Healthcare Mater.* **2020**, *9*, 1900951.
[26] T. Ghosh, B. Voit, N. Karak, *Polymer* **2020**, *200*, 122575.
[27] M. Cadena, L. Ning, A. King, B. Hwang, L. Jin, V. Serpooshan, S. A. Sloan, *Adv. Healthcare Mater.* **2021**, *10*, 2001600.
[28] Y. Yang, D. Lei, S. Huang, Q. Yang, B. Song, Y. Guo, A. Shen, Z. Yuan, S. Li, F.-L. Qing, X. Ye, Z. You, Q. Zhao, *Adv. Healthcare Mater.* **2019**, *8*, 1900065.
[29] H.-R. Lin, C.-J. Kuo, C. Y. Yang, S.-Y. Shaw, Y.-J. Wu, *J. Biomed. Mater. Res.* **2002**, *63*, 271.
[30] M. Rafiee, R. D. Farahani, D. Therriault, *Adv. Sci.* **2020**, *7*, 1902307.
[31] X. Wan, L. Luo, Y. Liu, J. Leng, *Adv. Sci.* **2020**, *7*, 2001000.
[32] J. E. Smay, J. Cesarano, J. A. Lewis, *Langmuir* **2002**, *18*, 5429.